Biosensors and Bioelectronics 184 (2021) 113227

Contents lists available at ScienceDirect

Biosensors and Bioelectronics

journal homepage: http://www.elsevier.com/locate/bios

A novel self-enhanced carbon nitride platform coupled with highly effective dual-recycle strand displacement amplifying strategy for sensitive photoelectrochemical assay

Qiao Ding, Minghui Zhu, Hanmei Deng, Ruo Yuan **, Yali Yuan *

Key Laboratory of Luminescence Analysis and Molecular Sensing, Ministry of Education, College of Chemistry and Chemical Engineering, Southwest University, Chongqing, 400715, PR China

ARTICLE INFO

Keywords:
Photoelectrochemical biosensor
Self-enhanced photoelectric active material
Dual-recycle TSD
miRNA-182-5p

ABSTRACT

In this work, a novel self-enhanced photoelectric active material, Na^+, K^+-codoped carbon nitride (NaKCN), was synthesized for constructing sensitive photoelectrochemical (PEC) biosensor to detect target miRNA-182-5p. Ingeniously, the NaKCN displayed glucose oxidase (GOx)-mimicking photocatalytic property, which catalyzed glucose to in situ generate high levels of H_2O_2 as its own electron donor for enhancing photocurrent. Moreover, the Na^+, K^+ co-doping could reduce energy gap of carbon nitride material, effectively improving the optical absorptivity and photocatalytic efficiency. Additionally, a novel highly effective dual-recycle TSD amplifying strategy was constructed to convert a small amount of target into plentiful two types of output DNAs labeling with sensitizer MB to enhance photocurrent of NaKCN. As a result, this PEC biosensor achieved a high sensitivity with low detection limit of 3.3 fM, which provided a new avenue for improving sensitivity of bioanalysis and diagnosis of diseases.

1. Introduction

Photoelectric active carbon nitride (g-C_3N_4), readily prepared by one-step polymerization of precursor materials like thiourea, melamine and dicyandiamide (Wang et al., 2016; Wang et al., 2019; Yan et al., 2019), is widely served as a signal probe to construct photoelectrochemical (PEC) sensors for detecting proteins, small molecules and miRNAs (Chen et al., 2020a; Jin et al., 2019; She et al., 2020; Zhang et al., 2012). Nevertheless, its intrinsic drawbacks, such as low visible light utilization efficiency and high photoelectron recombination rate, may bring in the imperative addition of electron donor/acceptor (D/A) in detection buffer to amplify photocurrent owing to the inferior photoelectric conversion efficiency (Chen et al., 2020b; Han et al., 2021a,b; Marci et al., 2019). Evidently, the common D/A including hydrogen peroxide (H_2O_2), ascorbic acid (AA) is prone to decomposition and move far away from photomaterials, thus influencing the analysis accuracy and sensitivity to a certain extent (Sun et al., 2019; Wang et al., 2018a). To be resolved, modifying g-C_3N_4 with the function of in situ generating its own electron donors derived from stable catalytic substrate (termed as self-enhanced photomaterial) is greatly significant (Ding et al., 2021; Tong et al., 2020; Yang et al., 2019), which not only shortens their mutual electron transfer distance, but also increases the local electron donor concentration (Sengupta et al., 2020; Wang et al., 2018b; Zhang et al., 2019). Here, we synthesized a novel Na^+, K^+ co-doped g-C_3N_4 (NaKCN) with glucose oxidase (GOx)-mimicking photocatalytic activity. The stable glucose could be photocatalyzed to in situ generation of high levels of H_2O_2 as electron donor toward NaKCN in the dissolved oxygen coexisted solution. What's more, the Na^+, K^+ evoked the improvement of visible light absorption, providing an ideal photoelectric active material for constructing highly accurate and sensitive PEC analysis system.

MiRNA-182-5p is a single-stranded RNA with 24 nucleotides, the high expression of which in the human body is related to colon cancer (Yan et al., 2020). Thus, it is of extremely vital significance to establish a simple, rapid and sensitive miRNA-182-5p detection method for colon cancer prevention and control. The toehold-mediated strand displacement (TSD) reaction has been known as one of most potential DNA signal amplification strategies because it is not restricted to nucleases and inherits desirable amplifying ability and specificity (Egloff et al., 2021; Han et al., 2021a,b; Saisuk et al., 2019). For TSD-induced single/dual-recycle amplifying analysis system, the target miRNA or DNA

* Corresponding author.
** Corresponding author.
E-mail addresses: yuanruo@swu.edu.cn (R. Yuan), y198688@swu.edu.cn (Y. Yuan).

https://doi.org/10.1016/j.bios.2021.113227
Received 21 February 2021; Received in revised form 2 April 2021; Accepted 5 April 2021
Available online 8 April 2021

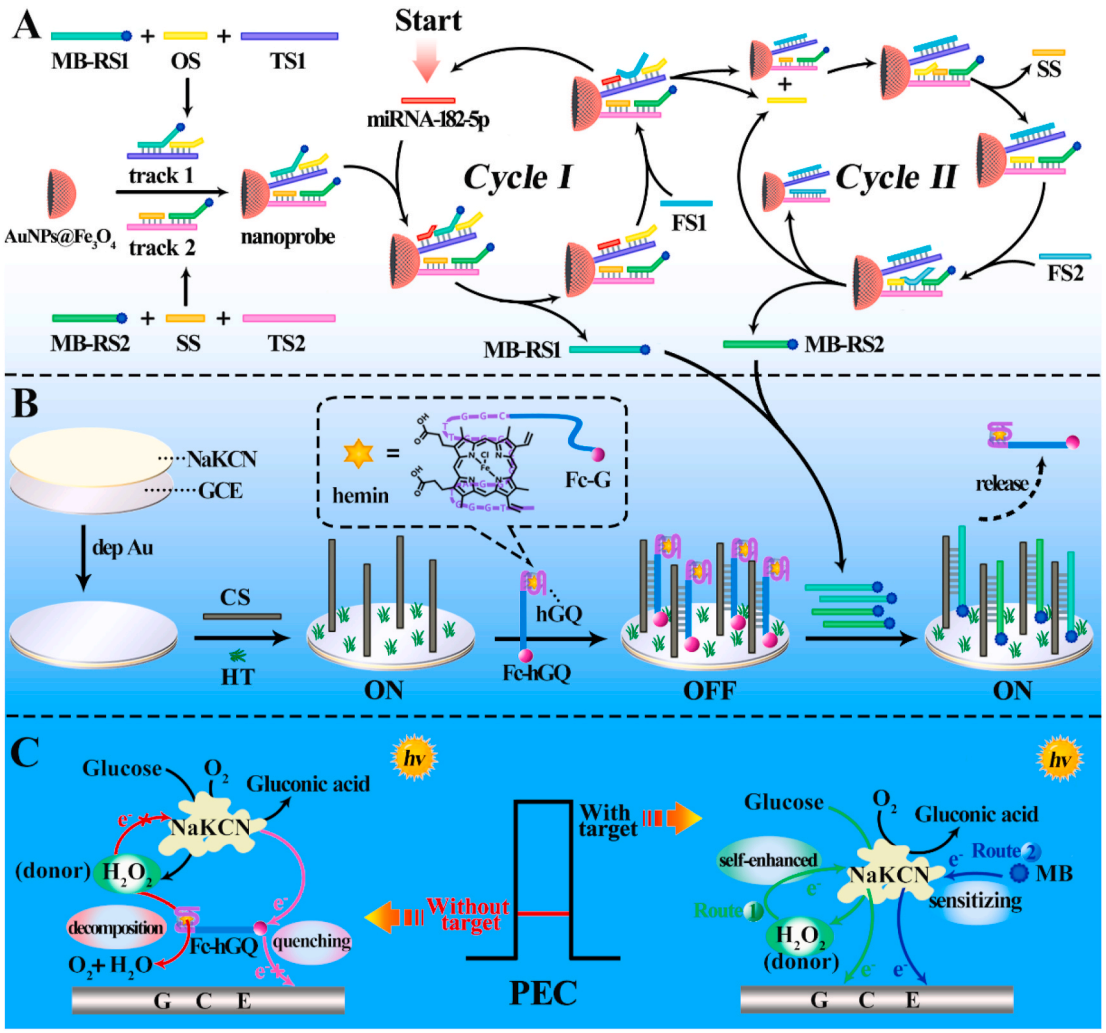

Scheme 1. Schematic diagrams of sensitive PEC biosensor for miRNA-182-5p assay: (A) the novel highly effective dual-recycle TSD amplification, (B) construction of on-off-on PEC biosensor, and (C) mechanism of photocurrent generating, quenching and enhancing.

with a small amount endows the hybridization with a short single-stranded overhanging region (the toehold) of DNA for displacing one or more prehybridized strands through a branch migration process, thereby ultimately generating many displaced strands as output DNAs in the assistant of other DNA strand for target recycling (Chu et al., 2018; Li et al., 2020). To be sure, the displaced strand is vital for target conversion efficiency and yet not fully utilized in most of reported works owing to the direct production of just only one type of useful output DNAs (Kong et al., 2019). Inspired by this, we designed a novel dual-recycle amplifying reaction that can consecutively produce two types of labeled output DNAs, neatly resolving the inferior target conversion efficiency in traditional TSD-induced amplifying analysis system by improving the utilization of assistant strand.

Based on the observation mentioned above, in this work, the multifunctional NaKCN was synthesized and served as sensing platform for constructing ultrasensitive PEC biosensor for miRNA182-5p assay, by coupling with the TSD-induced dual-recycle amplifying strategy. As depicted in Scheme 1, the self-enhanced NaKCN on electrode mimicked GOx activity and generated extremely high PEC signal in the present of glucose. However, the short DNA strand (Fc-G) with quencher ferrocene (Fc) could form hemin/G-quadruplex at terminals to obtain Fc-hGQ. The further decoration of Fc-hGQ leaded to a significantly decreased PEC signal because the Fc offered quenching effect and hemin/G-quadruplex (Chen et al., 2021; Golub et al., 2016) decomposed photocatalytic electron donor H_2O_2 generated by NaKCN. Then, the designed TSD-induced dual-recycle amplifying reaction with high target conversion efficiency consecutively produced two types of sensitizer methylene blue (MB) labeled output DNAs (MB-RS), which thus effectively released the Fc-hGQ for reactivating self-enhancement of NaKCN with recovered signal related to target concentration. Moreover, the sensitizer MB closed to NaKCN can further enhance the signal with improved detection sensitivity. Therefore, the detection system with high sensitivity realized multiple signal amplification by highly effective TSD-induced dual-recycle amplifying combining with MB sensitized self-enhanced NaKCN.

2. Experiment

The Materials and reagents, Instruments applied in this study were shown in the Supplementary Materials.

2.1. Synthesis of multifunctional bi-track@AuNPs@Fe_3O_4 nanoprobe

First, 5 mL 16 nm prepared AuNPs (Xia et al., 2020) were subjected into 200 μL amino-modified magnetic bead (NH_2–Fe_3O_4) solution with reaction of 12 h at 4 °C. After removing residual AuNPs by magnetic separation, the precipitate AuNPs@Fe_3O_4 was dispersed in 5 mL tris-HCl buffer. Meanwhile, the DNA bi-track composed of track 1 and track 2 were produced by follows: the reporter strand 1 labeled with MB (MB-RS1), output strand (OS), template strand 1 (TS1), supporting strand (SS), reporter strand 2 labeled with MB (MB-RS2) and template

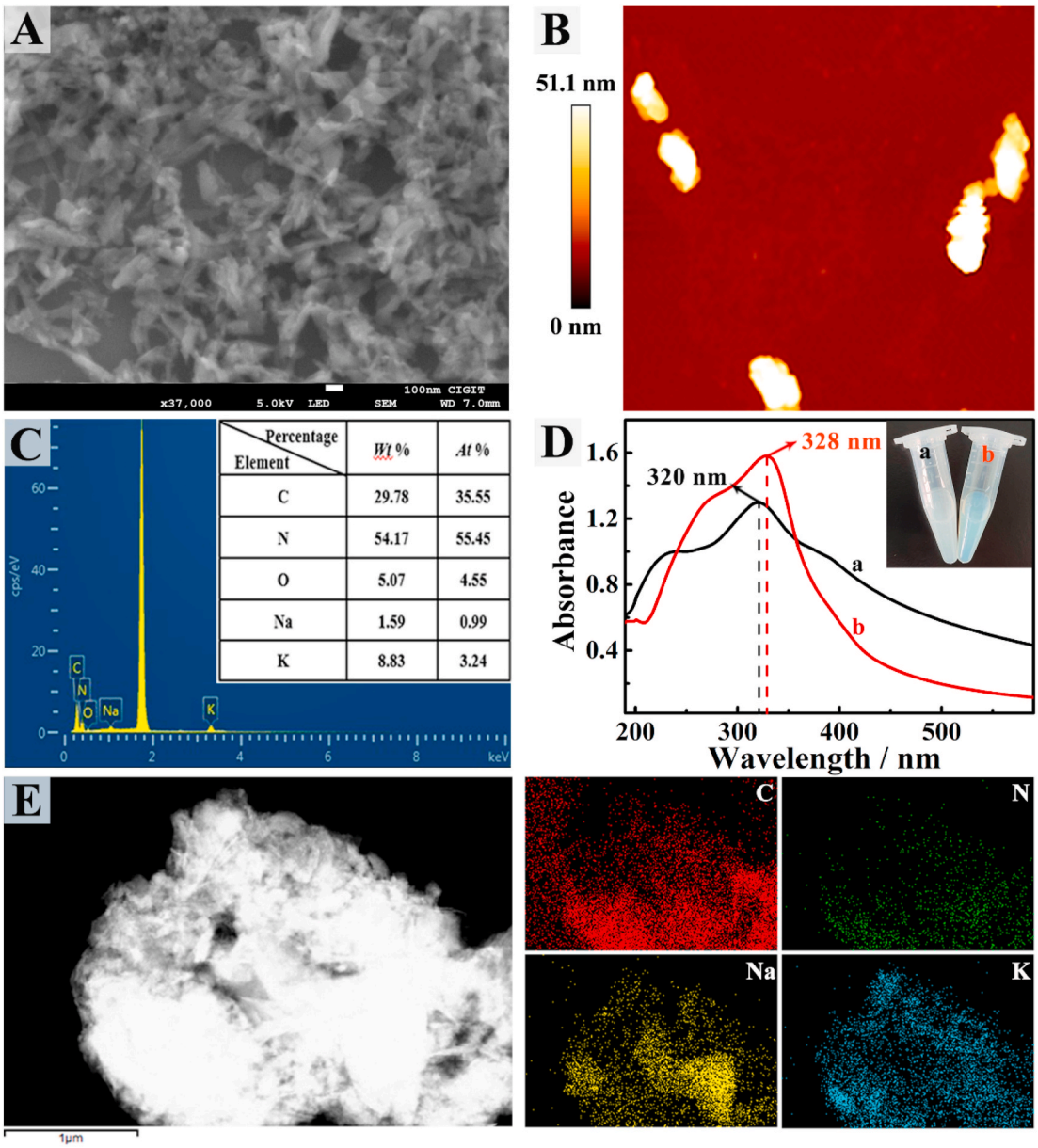

Fig. 1. (A) SEM and (B) AFM images of NaKCN. (C) The EDS analysis spectrogram of NaKCN. (D) The UV–Vis adsorption spectrums of (a) g-C_3N_4 and (b) NaKCN (insert: photographs of g-C_3N_4 and NaKCN dispersed in water). (E) The HADDF-STEM and corresponding EDS mapping of C, N, Na and K elements in NaKCN. (For interpretation of the references to color in this figure legend, the reader is referred to the Web version of this article.)

strand 2 (TS2) were firstly heated at 95 °C for 5 min and slowly cooled to 25 °C. Then 20 μL 2 μM MB-RS1, OS and TS1 were reacted at 37 °C for 2 h to form the track 1. The analogous synthetic route was available for track 2, which synthesized by 20 μL 2 μM SS, MB-RS2 and TS2. Subsequently, 480 μL AuNPs@Fe_3O_4 was added into the mixture of track 1 and track 2 for the reaction of 12 h at 4 °C. Track 1 and track 2 with –SH terminal could be co-immobilized on AuNPs@Fe_3O_4 surface owing to the S–Au binding, forming the expected bi-track@AuNPs@Fe_3O_4 nanoprobe. Further, the superfluous strands were removed by magnetic separation and the as-obtained bi-track@AuNPs@Fe_3O_4 nanoprobe was dispersed with 150 μL tris-HCl buffer and stored at 4 °C for subsequent experiment.

2.2. Highly effective dual-recycle TSD amplification strategy

For significantly enhancing the sensitivity of miRNA-182-5p detection, we designed the novel highly effective dual-recycle TSD amplification that obtained substantial output DNAs, and the corresponding principle was illustrated in Scheme 1. Once 10 μL target miRNA-182-5p was subjected to 10 μL prepared bi-track@AuNPs@Fe_3O_4 nanoprobe solution, MB-RS1 on track 1 was replaced by miRNA-182-5p and entered to solution. After introducing 8 μL 6 μM fuel strand 1 (FS1), the miRNA-182-5p and OS was displaced by FS1. The released miRNA-182-5p was recycling in cycle I and released OS initiated cycle II by replacing SS on track 2. Through adding 8 μL 6 μM fuel strand 2 (FS2), MB-RS2 on track 2 was also released into solution. Here, the MB-RS could combine with capture strand (CS) on electrode surface. Thus, an ingenious dual-recycle amplification with high target conversion efficiency was acquired for outputting substantial MB labeled DNAs.

2.3. Fabrication of PEC biosensor

First, 10 μL NaKCN was dropped onto the pretreated glassy carbon

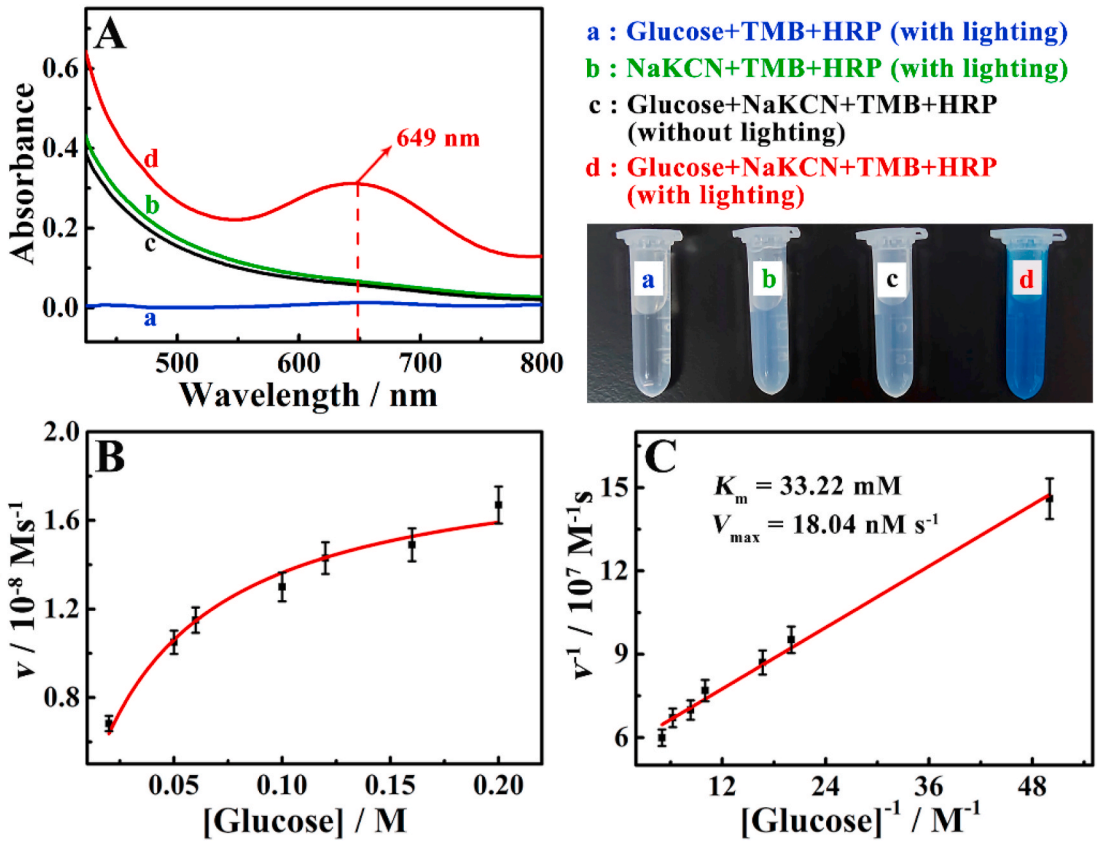

Fig. 2. (A) UV–Vis spectra and changing color picture of (a) Glucose + TMB + HRP, (b) NaKCN + TMB + HRP, (c) Glucose + NaKCN + TMB + HRP (without lighting) and (d) Glucose + NaKCN + TMB + HRP (with lighting). Steady-state kinetic assay of GOx-mimicking activity: the velocity (ν) in Michaelis-Menten curve (B) was measured by absorbance of reaction with various concentration of glucose and the Lineweaver–Burk double reciprocal plots (C). (For interpretation of the references to color in this figure legend, the reader is referred to the Web version of this article.)

electrode (GCE) (Tian et al., 2020) and dried at 37 °C to form an uniform layer. Then, the NaKCN/GCE was dipped into *wt* 1% $HAuCl_4$ solution for electrodeposition of AuNPs (depAu) to obtain depAu/NaKCN/GCE. Following that, 10 μL 2 μM CS was incubated onto the electrode and reacted at 4 °C for 12 h. Subsequently, 10 μL 0.1 mM hexanethiol (HT) with incubation time of 40 min was utilized for blocking the non-specific adsorption. Afterward, 10 μL mixture containing equal volume of 10 μM hemin and 4 μM Fc-G was dropped on HT/CS/depAu/NaKCN/GCE for reaction of 2 h at 37 °C, aiming at decorating Fc-hGQ on electrode to form the Fc-hGQ/HT/CS/depAu/NaKCN/GCE. Finally, 10 μL MB-RS solution from dual-recycle TSD amplification was incubated on modified electrode for reacting 2 h at 37 °C, during which the quencher Fc-hGQ was removed while sensitizer MB labeled DNA was decorated on the modified electrode.

3. Discussion

3.1. Morphology and component characterization of NaKCN

To characterize the size and morphology of NaKCN, the scanning electron microscopy (SEM) and atomic force microscopy (AFM) were carried out. The SEM images of NaKCN was shown in Fig. 1A, the NaKCN exhibited slightly loose structure made up of irregular lumps connected and stacked, which mainly due to the doping of K^+ and Na^+ (Zhang et al., 2020). In the AFM image of Fig. 1B, the morphology of NaKCN was consistent with Fig. 1A and the height was about 50 nm. The corresponding energy-dispersive X-ray spectroscopy (EDS) analysis was illustrated in Fig. 1C, exhibiting the successful doping of K^+ and Na^+ into the g-C_3N_4. Fig. 1D was the UV–vis absorption of g-C_3N_4 and NaKCN, g-C_3N_4 exhibited a strong absorption peak at 320 nm. While the absorption peak appeared a redshift and changed to 328 nm after the K^+ and Na^+ doping into it, indicating that K^+ and Na^+ reacted with amino species of g-C_3N_4 to form N–K bond and N–Na bond, could connect more tri-*s*-triazine rings to form a larger conjugated system. In the insert of Fig. 1D, a and b showed the colors of g-C_3N_4 and NaKCN dispersed in water. The high-angle annular dark-field scanning transmission electron microscopy (HADDF-STEM) image and EDS mapping images were shown in Fig. 1E, it revealed that there appears a distribution of C, N, Na and K across the structure of NaKCN. Among this, the Na and K elements were detected in the entire structure, verifying the introduction and homogeneous dispersion of Na and K elements in g-C_3N_4.

3.2. GOx-like activity of NaKCN

Here, UV–vis absorption spectroscopy was used to verify the GOx-mimicking photocatalytic activity of NaKCN. The catalytic process could be well described by the typical Michaelis–Menten model. In the acetate buffer solution (0.2 M, pH 3.5), horseradish peroxidase (HRP) could oxidize 3,3',5,5'-tetramethylbenzidine (TMB) to blue oxTMB in the presence of H_2O_2 (Jiang et al., 2016; Liu et al., 2020). As shown in Fig. 2A, after visible light irradiation at 400 nm, the UV–vis absorption spectra of TMB and HRP mixing with glucose (curve a) and NaKCN (curve b) had little absorption at 649 nm, respectively. The spectra of mixture of glucose, NaKCN, TMB and HRP in the absence of irradiation (curve c) also showed a little absorption at 649 nm while that of same mixture after irradiation (curve d) exhibited an obvious absorption peak. The above results were consistent with the color changes of various mixtures in the right photograph of Fig. 2A. In the presence of glucose (a) or NaKCN (b), the mixture solution of TMB and HRP was colorless after irradiation. The mixture solution of TMB, HRP, glucose

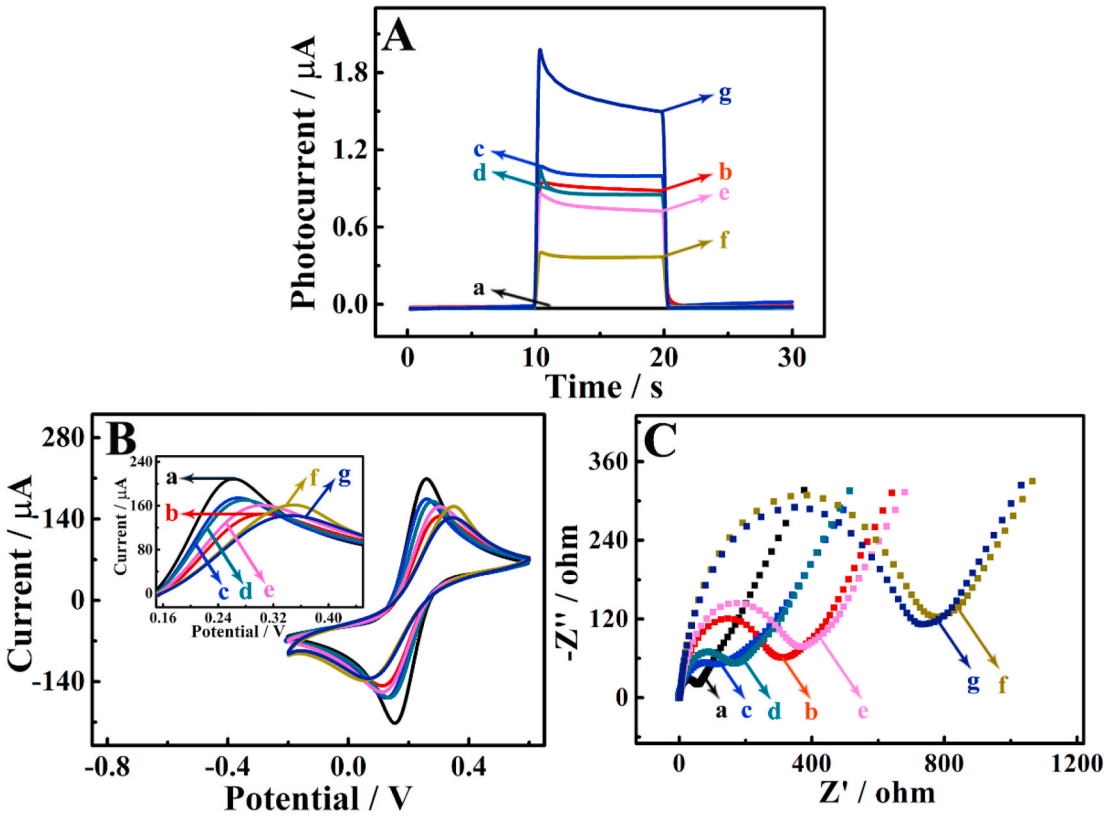

Fig. 3. (A) PEC, (B) CV and (C) EIS responses of (a) bare GCE, (b) NaKCN/GCE, (c) depAu/NaKCN/GCE, (d) CS/depAu/NaKCN/GCE, (e) HT/CS/depAu/NaKCN/GCE, (f) Fc-hGQ/HT/CS/depAu/NaKCN/GCE and (g) MB-RS/HT/CS/depAu/NaKCN/GCE.

and NaKCN exhibited colorless in the absence of irradiation (c) and blue after irradiation (d), respectively. Thus, NaKCN could mimic GOx after visible light irradiation to generate H_2O_2 in situ. Besides, the comparison of GOx-like activity of NaKCN and g-C_3N_4 was shown in Fig. S1A. The absorption of mixture of glucose, TMB, HRP and NaKCN at 649 nm was markedly higher than that of g-C_3N_4, which illustrated that NaKCN had an excellent GOx-like activity in comparing with g-C_3N_4.The Michaelis-Menten curve (Fig. 2B) showed the relationship between glucose concentration and initial velocity (ν) calculated from dynamic data. To obtain the maximum initial velocity (V_{max}) and Michaelis–Menten constant (K_m), the Lineweaver–Burk double reciprocal plots (Fig. 2C) was made from Michaelis-Menten curve according to $\nu = V_{max}[S]/(K_m + [S])$. The slopes and intercepts of fitted line could give out the value of V_{max} and K_m, and the corresponding K_m value of NaKCN using glucose as a substrate was 33.22 mM. In conclusion, NaKCN possessed outstanding photocatalytic efficiency towards glucose.

3.3. PEC and electrochemical characterization of the biosensor fabrication

In order to verify the feasibility of biosensor fabrication, the stepwise construction process was confirmed by PEC and electrochemical characterization. Fig. 3A showed PEC response of each step modified electrode. Comparing with the photocurrent of bare GCE (curve a), NaKCN modified electrode showed an obvious photocurrent attributing to not only the intrinsic photoactive but also the in situ generated H_2O_2 by self-photocatalysis of NaKCN (curve b). When conductive depAu was coated on NaKCN modified electrode, an increased photocurrent could be acquired (curve c). After continuous immobilization inert CS (curve d) and HT (curve e), photocurrent decreased continually (curve d and curve e). Subsequently, the modification of Fc-hGQ with quenching effect on electrode caused a significantly decreased photocurrent (curve f). Finally, the MB-RS from dual-recycle TSD amplification displaced Fc-hGQ, which enabled the corresponding photocurrent recover and further enhance, ascribing to the remove of Fc-hGQ and sensitization of MB (curve g).

Moreover, the electrochemical measurement including cyclic voltammetry (CV) and electrochemical impedance spectroscopy (EIS) were also used to further verify the assembly procedures of fabricated electrode. The inset with zoom on the redox peaks of CV curves was added in Fig. 3B. From the inset of Fig. 3B and C, the bare GCE showed a well defined redox peak and a small resistance (R_{et}) response (curve a), while the NaKCN/GCE showed a decreased peak current and an increased R_{et} response owing to its effect of hindering electron transfer (curve b). When depAu was coated on modified electrode, an obvious increase of peak current and decreased R_{et} response was observed because of the excellent conductivity of depAu (curve c). Subsequently, the peak current decreased sequentially while R_{et} response increased continually for the incubation of CS (curve d) and HT (curve e), which attributed to the electrostatic repulsion of nucleotide sequences and the inhibition of HT. After modifying Fc-hGQ, the R_{et} response increased significantly owing to the electronic repulsion of nucleotide sequences, while the redox peak current barely changed attributing to the electroactive Fc (curve f). After MB-RS displacing Fc-hGQ, a decrease of peak current was obtained because the release of electroactive Fc. The R_{et} response also decreased, which was attributed to the weaker electronic repulsion of shorter nucleotide sequences MB-RS (curve g). Furthermore, the redox peak of CV curves roughly showed continuous positive shift as the different layers were modified on the electrode except curve b, which ascribed to the different extent polarization phenomenon caused by the each step of modified electrode with different charges. Furthermore, the positive shift of the redox peak could also indicate that the electrode material had better catalytic activity. When modified with NaKCN (curve b) and Fc-hGQ (curve f) on the electrode, the significant positive shift of redox peak demonstrated the enzyme-mimicking properties of them.

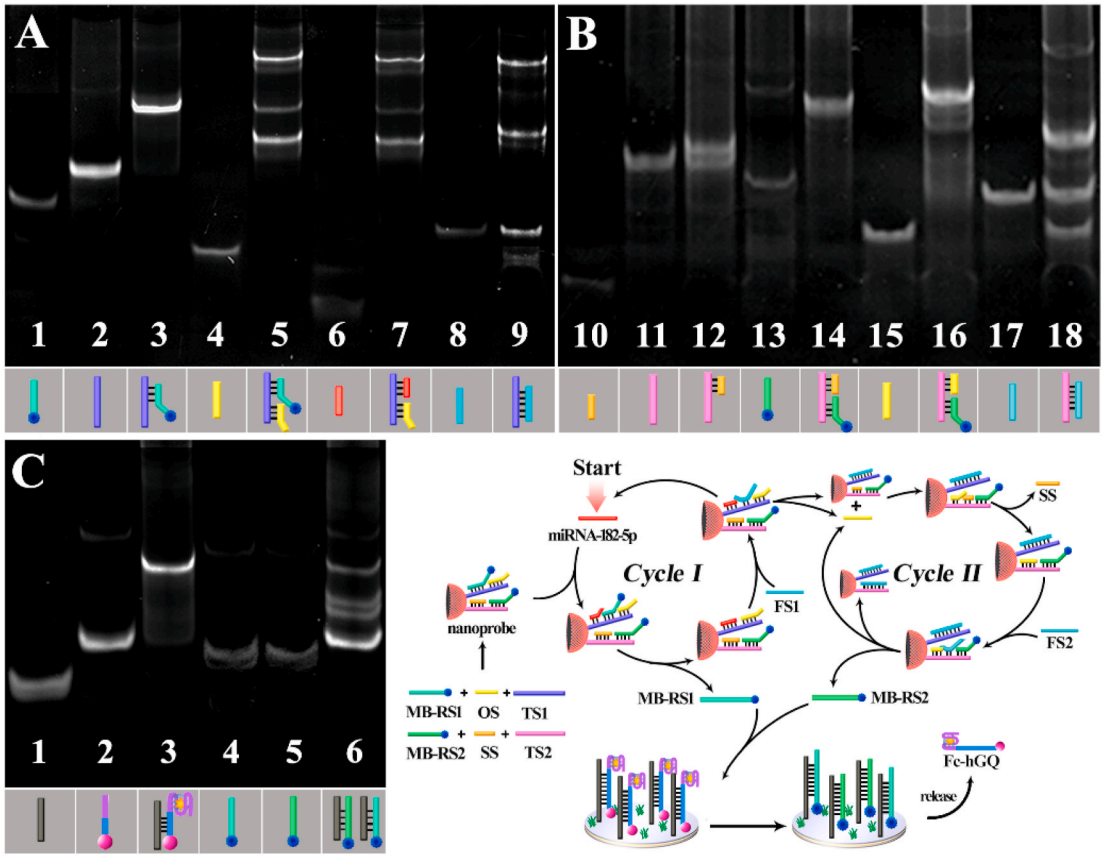

Fig. 4. PAGE analysis: (A) Cycle I: lane 1, MB-RS1; lane 2, TS1; lane 3, MB-RS1+TS1; lane 4, OS; lane 5, track 1; lane 6, miRNA-182-5p; lane 7, track 1+miRNA-182-5p; lane 8, FS1; lane 9, track 1+miRNA-182-5p + FS1. (B) Cycle II: lane 10, SS; lane 11, TS2; lane 12, SS + TS2; lane 13, MB-RS2; lane 14, track 2; lane 15, OS; lane 16, track 2+OS; lane 17, FS2; lane 18, track 2+ OS + FS2. (C) Electrode surface: lane 1, CS; lane 2, Fc-hGQ; lane 3, CS + Fc-hGQ; lane 4, MB-RS1; lane 5, MB-RS2; lane 6, CS + Fc-hGQ + MB-RS1+MB-RS2.

3.4. Polyacrylamide gel electrophoresis (PAGE) characterization of dual-recycle TSD amplification reaction and biosensor fabrication

The PAGE was performed to verify the successful dual-recycle TSD amplification reaction and biosensor construction. The PAGE result of reaction process of cycle I was shown in Fig. 4A, single band of lane 1 and lane 2 presented MB-RS1 and TS1, respectively. The band of lane 3 with slower migration than lane 1 and lane 2 was the hybridization product of MB-RS1 and TS1. After adding OS (lane 4) into the former mixture, the top band of lane 5 migrated slower than the band of lane 3 owing to the hybridization of MB-RS1 and TS1 with OS (track 1). When adding miRNA-182-5p (lane 6) into track 1, the top band of lane 7 was the hybridization of miRNA-182-5p, OS and TS1 with faster speed, suggesting that target successfully displaced MB-RS1 and thus triggered the cycle I. When the FS1 (lane 8) was added to the mixture of lane 7, the lane 9 expressed four bands. The top band was the excessive hybridization product of miRNA-182-5p, OS and TS1. The second band migrated faster implied that FS1 hybridized with TS1 successfully to form the hybrid structure of FS1 and TS1 while displacing miRNA-182-5p and OS. The third band and bottom band presented excessive FS1 and released OS, respectively. The above results demonstrated the recycling of target. Similarly, the reaction process of cycle II was displayed in Fig. 4B, the band of lane 10 and lane 11 presented single strand SS and TS2. The hybrid structure from the hybridization of SS with TS2 was observed in lane 12, which continue to hybridize with MB-RS2 (lane 13) to form track 2 exhibiting in the lane 14. With addition of OS (lane 15), the band of lane 16 exhibited slower migration speed than lane 14 on account of the displacement of SS from track 2 by OS. When the FS2 (lane 17) was added into the previous mixture, the top band of lane 18 moved faster than the band of lane 16, owing to the release of OS and MB-RS2. As shown in Fig. 4C, lane 1 and lane 2 was PAGE results of CS and Fc-hGQ, respectively. The band of lane 3 migrated slower than the band of CS and Fc-hGQ due to the successful hybridization of CS and Fc-hGQ. After adding MB-RS1 (lane 4) and MB-RS2 (lane 5) into the mixture of CS and Fc-hGQ, four bands could be seen in lane 6, which represented the excessive hybridization product of CS with Fc-hGQ, hybridization product of MB-RS1 and MB-RS2 with CS, the released Fc-hGQ from top to bottom, respectively.

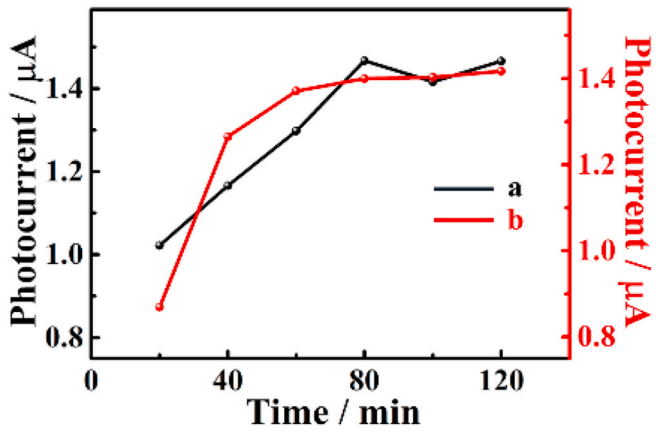

Fig. 5. Experiment conditions were optimized by PEC measurement: (a) the reaction time of dual-recycle TSD amplification and (b) incubation time of signal probes on the electrode surface.

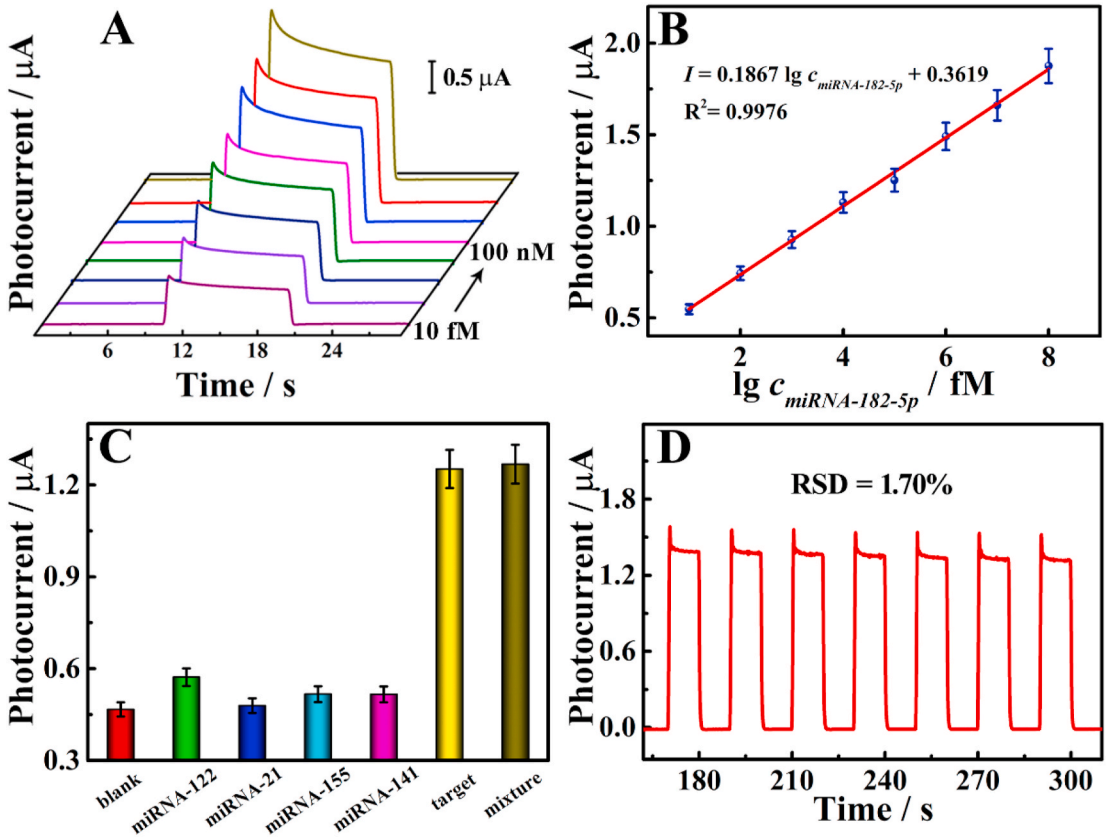

Fig. 6. (A) Photocurrent of the constructed biosensor toward various concentrations of miRNA-182-5p: 10 fM, 100 fM, 1 pM, 10 pM, 100 pM, 1 nM, 10 nM, and 100 nM. (B) The calibration curve for detection of target. (C) Selectivity analysis: photocurrent of biosensor toward 0.1 nM miRNA-182-5p, 10 nM miRNA-122, miRNA-21, miRNA-155 and miRNA-141, and the mixture. (D) Stability of biosensor (100 pM miRNA-182-5p) under continuous off–on–off light.

3.5. Optimization of experiment conditions

The reaction time of dual-recycle TSD amplification and signal probes on electrode surface had an obvious influence in performance of PEC biosensor. According to the experiment of dual-recycle TSD amplification, the miRNA-182-5p (100 pM), FS1, FS2 and prepared bi-track@AuNPs@Fe_3O_4 nanoprobe solution were mixed and reacted at 37 °C for 20 min, 40 min, 60 min, 80 min, 100 min and 120 min, respectively. After that, the signal probes MB-RS solution obtained by magnetic separation from corresponding mixtures were incubated on Fc-hGQ/HT/CS/depAu/NaKCN/GCE for 2 h at 37 °C to measure photocurrent. The optimization results were displaced in Fig. 5. The photocurrent (curve a) increased significantly with longer reaction time and reached the maximum value at 80 min, so reaction time of 80 min was selected as the optimal reaction time of dual-recycle TSD amplification. Analogously, after dual-recycle TSD amplification reacting for the optimal time, the incubation time of MB-RS solution from dual-recycle TSD amplification on Fc-hGQ/HT/CS/depAu/NaKCN/GCE was also optimized (20 min, 40 min, 60 min, 80 min, 100 min and 120 min). The photocurrent (curve b) increased continuously with longer time and reached a plateau at 80 min, so we selected 80 min incubation time of signal probes.

3.6. Analytical performance of proposed biosensor

At the optimal experimental conditions, the performance of proposed biosensor was investigated with various concentrations of target. Seen from Fig. 6A and B, the photocurrent (I) increased gradually with the increased logarithm of concentration of target (lg $c_{miRNA\text{-}182\text{-}5p}$) in the range from 10 fM to 100 nM and lg $c_{miRNA\text{-}182\text{-}5p}$ was linear with I. The regression equation was $I = 0.1867 \lg c_{miRNA\text{-}182\text{-}5p} + 0.3619$ ($R^2 = 0.9976$). The detection limit for target concentration was estimated to be 3.3 fM (S/N = 3). Thus, the excellent amplification efficiency of dual-recycle TSD amplification resulted in the high sensitivity and wide linear range of biosensor.

3.7. Selectivity, stability, and application of the biosensor

The selectivity of fabricated biosensor was evaluated by detecting miRNA-182-5p (0.1 nM), other interfering miRNAs (10 nM), including miRNA-122, miRNA-21, miRNA-155 and miRNA-141, and the mixture of all previous miRNAs. As shown in Fig. 6C, the photocurrent of miRNA-182-5p and mixture were obviously higher than that of other interfering miRNAs and blank sample, which manifested that the proposed biosensor had good selectivity for miRNA-182-5p detection. Meanwhile, the stability of constructed biosensor was verified by continuous scanning towards 100 pM miRNA-182-5p under a continually periodical "off-on-off" light for seven cycles. The corresponding relative standard deviation (RSD) was 1.70% (Fig. 6D), which implied that the constructed biosensor possessed acceptable stability. In addition, standard addition method was used to evaluate the feasibility of the biosensor. Specifically, the photocurrent with different concentrations of miRNA182-5p (10 fM, 100 fM, 1 pM, 100 pM) diluted with 50 times healthy human serum was detected, and the calculated recovery and RSD ranged from 96.49 to 107.8% and 2.6 to 4.2%, respectively. The obtained results had no distinct deviation between the actual test and the theoretical addition amount, which proved that the PEC biosensor possessed an excellent potential application in clinical research.

4. Conclusions

In summary, we constructed an ultrasensitive PEC biosensor for

miRNA-182-5p determination in terms of functional NaKCN coupling with a novel highly effective dual-recycle TSD amplification strategy. Specifically, NaKCN was manifested as self-enhanced material by catalyzing the oxidation of glucose to in situ generate its own electron donor H_2O_2 under visible irradiation. Besides, the plentiful output DNAs labeled with sensitizer MB releasing from dual-recycle TSD amplification could further enhance PEC signal, thus effectively improving detection sensitivity. In brief, the proposed biosensor with facile and efficient signal amplification exhibited a new perspective for sensitive bioanalysis.

CRediT authorship contribution statement

Qiao Ding: Conceptualization, Data curation, Formal analysis, Investigation, Writing – original draft, Writing – review & editing. **Minghui Zhu:** Data curation, Investigation. **Hanmei Deng:** Conceptualization, Writing – original draft, Supervision. **Ruo Yuan:** Conceptualization, Writing – original draft, Supervision. **Yali Yuan:** Funding acquisition, Resources, Writing – review & editing.

Declaration of competing interest

The authors declare that they have no known competing financial interests or personal relationships that could have appeared to influence the work reported in this paper.

Acknowledgments

This work was supported by the Fundamental Research Funds for the Central Universities (XDJK2020TY002, XDJK2019B022), the National Natural Science Foundation (NNSF) of China (51473136, 21575116).

Appendix A. Supplementary data

Supplementary data to this article can be found online at https://doi.org/10.1016/j.bios.2021.113227.

References

Chen, D., Wang, X.H., Zhang, K.Z., Cao, Y., Tu, J.C., Xiao, D., Wu, Q., 2020a. Biosens. Bioelectron. 166, 112466.
Chen, J.L., Yan, J., Feng, Q.M., Miao, X.M., Dou, B.T., Wang, P., 2021. Biosens. Bioelectron. 176, 112955.
Chen, Y.F., Jiao, L., Yan, H.Y., Xu, W.Q., Wu, Y., Wang, H.J., Gu, W.L., Zhu, C.Z., 2020b. Anal. Chem. 92, 13518–13524.
Chu, Y.X., Wu, R., Fan, G.C., Deng, A.P., Zhu, J.J., 2018. Acs Sustain Chem. Eng. 6, 11633–11641.
Ding, H., Hu, B., Zhang, B., Zhang, H., Yan, X.Y., Nie, G.H., Liang, M.M., 2021. Nano Res 14, 570–583.
Egloff, S., Melnychuk, N., Reisch, A., Sophie, M., Andrey, S.K., 2021. Biosens. Bioelectron. 179, 113084.
Golub, E., Albada, H.B., Liao, W.C., Biniuri, Y., Willner, I., 2016. J. Am. Chem. Soc. 138, 164–172.
Han, B., Sha, L.J., Yu, X.M., Yang, M., Cao, Y., Zhao, J., 2021a. Biosens. Bioelectron. 176, 112913.
Han, F.J., Song, Z.Q., Xu, J.N., Dai, M.J., Luo, S.L., Han, D.X., Niu, L., Wang, Z.X., 2021b. Biosens. Bioelectron. 177, 112978.
Jiang, X.Y., Geng, F.H., Wang, Y.X., Liu, J.H., Qu, P., Xu, M.T., 2016. Biosens. Bioelectron. 81, 268–273.
Jin, X., Chen, J.L., Zeng, X.X., Xu, L.J., Wu, Y.N., Fu, F.F., 2019. Biosens. Bioelectron. 128, 45–51.
Kong, Y.C., Liu, X.W., Liu, C.X., Xue, Q.W., Li, X., Wang, H.S., 2019. Analyst 144, 4694–4701.
Li, J., Weng, X., Mo, F., Han, M., Li, H.B., 2020. Anal. Chem. 92, 15145–15151.
Liu, S.J., Dou, L.N., Yao, X.L., Zhang, W.T., Zhao, M., Yin, X.C., Sun, J., Zhang, D.H., Wang, J.L., 2020. Biosens. Bioelectron. 169, 112610.
Marci, G., Garcia-Lopez, E.I., Pomilla, F.R., Palmisano, L., Zaffora, A., Santamaria, M., Krivtsov, I., Ilkaeva, M., Barbierikova, Z., Brezova, V., 2019. Catal. Today 328, 21–28.
Saisuk, W., Srisawat, C., Yoksan, S., Dharakul, T., 2019. Anal. Chem. 91, 3286–3293.
Sengupta, P., Pramanik, K., Datta, P., Sarkar, P., 2020. Biosens. Bioelectron. 154, 112072.
She, Y.M., Tam, R.Y., Li, X.G., Rosu-Myles, M., Sauve, S., 2020. Anal. Chem. 92, 14038–14046.
Sun, H.B., Xu, W., Liu, B., Liu, Q.R., Wang, Q.W., Li, L.Z., Kong, J.M., Zhang, X.J., 2019. Anal. Chem. 91, 9198–9205.
Tian, B.W., Zhao, L.X., Li, R., Zhai, T.T., Zhang, N.N., Duan, Z.M., Tan, L., 2020. Anal. Chem. 92, 15916–15926.
Tong, Y.W., Wei, C.G., Li, Y., Zhang, Y.F., Lin, W., 2020. Phys. Chem. Chem. Phys. 22, 21099–21107.
Wang, B., Mei, L.P., Ma, Y., Xu, Y.T., Ren, S.W., Cao, J.T., Liu, Y.M., Zhao, W.W., 2018a. Anal. Chem. 90, 12347–12351.
Wang, X.J., Feng, J., Bai, Y.C., Zhang, Q., Yin, Y.D., 2016. Chem. Rev. 116, 10983–11060.
Wang, Y.Y., Zhao, S., Zhang, Y.W., Fang, J.S., Zhou, Y.M., Yuan, S.H., Zhang, C., Chen, W.X., 2018b. Appl. Surf. Sci. 440, 258–265.
Xia, L.Y., Li, M.J., Wang, H.J., Yuan, R., Chai, Y.Q., 2020. Anal. Chem. 92, 14550–14557.
Yan, P.C., Dong, J.T., Mo, Z., Xu, L., Qian, J.C., Xia, J.X., Zhang, J.M., Li, H.N., 2019. Biosens. Bioelectron. 148, 111802-111802.
Yan, S.S., Wang, H., Chen, X.H., Liang, C.H., Shang, W.W., Wang, L., Li, J., Xu, D.H., 2020. Canc. Lett. 488, 18–26.
Yang, H.M., Hu, M.S., Li, Z.L., Zhao, P.N., Xie, L., Song, X.R., Yu, J.H., 2019. Anal. Chem. 91, 14577–14585.
Zhang, J.Z., Yu, C.Y., Lang, J.Y., Zhou, Y.F., Zhou, B.X., Hu, Y.H., Long, M.C., 2020. Appl. Catal., B 277, 119225.
Zhang, P., Sun, D., Cho, A., Weon, S., Lee, S., Lee, J., Han, J.W., Kim, D.P., Choi, W., 2019. Nat. Commun. 10, 940.
Zhang, Y.W., Liu, J.H., Wu, G., Chen, W., 2012. Nanoscale 4, 5300–5303.